Journal of Alloys and Compounds 480 (2009) 603–607

Contents lists available at ScienceDirect

Journal of Alloys and Compounds

journal homepage: www.elsevier.com/locate/jallcom

Improvement of optical properties of nanocrystalline Fe-doped ZnO powders through precipitation method from citrate-modified zinc nitrate solution

T. Rattana [a], S. Suwanboon [b,*], P. Amornpitoksuk [c], A. Haidoux [d], P. Limsuwan [a]

[a] Department of Physics, Faculty of Science, King Mongkut's University of Technology Thonburi, Bangkok 10140, Thailand
[b] Materials Science Program, Faculty of Science, Prince of Songkla University, Hat Yai, Songkhla 90112, Thailand
[c] Department of Chemistry, Faculty of Science, Prince of Songkla University, Hat Yai, Songkhla 90112, Thailand
[d] Institut Charles Gerhardt, UMR 5253, PMOF, Universite Montpellier 2, Place Eugene Bataillon, Montpellier 34095, Cedex 5, France

ARTICLE INFO

Article history:
Received 26 October 2008
Received in revised form 23 January 2009
Accepted 1 February 2009
Available online 12 February 2009

Keywords:
Nanostructured materials
Oxide materials
Precipitation
Optical properties
Luminescence

ABSTRACT

Nanocrystalline $Zn_{1-x}Fe_xO$ (where $x = 0$, 0.01 and 0.02) powders were successfully synthesized by a precipitation method from citrate-modified zinc nitrate solution. X-ray powder diffraction, Fourier transformed infrared spectroscopy, field emission scanning electron microscopy, transmission electron microscopy and energy dispersive spectroscopy were used to study the structural properties. The optical properties were determined by UV–vis spectrophotometer and luminescent spectrometer. In this study, the optical band gap of nanocrystalline ZnO powder increased from 3.170 eV to 3.214 eV when the Fe concentration in the solution was increased up to 2 mol. %.

1. Introduction

Recently, there has been a surge of interest in nanomaterials or nanostructured materials particularly metal oxide nanoparticles. To date, ZnO is an important wide band gap semiconductor and it has a prospect of widespread application in many fields owing to its outstanding optical and electronic properties. It is well known that the optical band gap of ZnO nanoparticles can be improved if its particle size decreased. Interestingly, there are two general routes to diminish a particle size of ZnO by a precipitation method. Firstly, the use of surfactant to modify the zinc precursor solution such as polyethylene glycol [1], diethanolamine (DEA) [2], triethanolamine (TEA) and cetyltrimethylammonium bromide (CTAB) [3] and secondly, the use of transition metal ions to substitute at Zn sites in the ZnO structure such as Al [4], Co [5], Mn [6] and Fe [7]. Nowadays, the preparation of nanocrystalline Fe-doped ZnO powders has been interesting because of its multifunctional material. Many studies had focused on its magnetic properties, whereas a few reports had concentrated on its optical properties. In this study, we report the influence of Fe concentration on the structural and optical properties of nanocrystalline $Zn_{1-x}Fe_xO$ ($x = 0$, 0.01 and 0.02) powders prepared from a citrate-modified zinc nitrate solution. The trisodium citrate dihydrate was chosen in this study because it can adsorb strongly on the surface of particle and significantly change the surface properties [8]. This study is the first attempt for using the trisodium citrate dihydrate to modify and stabilize nanocrystalline $Zn_{1-x}Fe_xO$ ($x = 0$, 0.01 and 0.02) powders prepared from a precipitation method at 70 °C.

2. Experimental

2.1. Materials

Zinc nitrate hexahydrate ($Zn(NO_3)_2{\cdot}6H_2O$, Fluka), trisodium citrate dihydrate ($Na_3C_6H_5O_7{\cdot}2H_2O$, RDH), iron (III) chloride hexahydrate ($FeCl_3{\cdot}6H_2O$, RDH) and sodium hydroxide (NaOH, Carlo Erba) are analytical grade and were used without further purification.

2.2. Synthesis of nanocrystalline ZnO powders

Nanocrystalline ZnO powders were precipitated from $Zn(NO_3)_2{\cdot}6H_2O$ solution in the presence of $Na_3C_6H_5O_7{\cdot}2H_2O$ acting as a surface modifying agent or stabilizer. Typically, 0.04 mol $Zn(NO_3)_2{\cdot}6H_2O$ was first dissolved in 100 mL of distilled water at room temperature. 0.04 mol $Na_3C_6H_5O_7{\cdot}2H_2O$ was then added into the above solution with continuous stirring until clear solution was obtained. Then, the citrate-modified $Zn(NO_3)_2{\cdot}6H_2O$ solution was stirred at 70 °C and finally 0.08 mol NaOH that was dissolved in 100 mL of distilled water was dropped slowly into the previous solution. The white precipitates were obtained and they were still stirred vigorously at 70 °C for 1 h. After being cooled to room temperature, these precipitates were filtered, rinsed with distilled water several times and ethanol, then collected and dried at 80 °C for 1 h, and finally calcined at 500 °C in air for 1 h. The calcination temperature was chosen at 500 °C because it is the lowest temperature to get rid of an impurity phase when considering from TGA analysis (it does not show here).

* Corresponding author. Tel.: +66 74 28 82 50; fax: +66 74 21 87 01.
E-mail address: ssumetha@yahoo.com (S. Suwanboon).

0925-8388/$ – see front matter © 2009 Elsevier B.V. All rights reserved.
doi:10.1016/j.jallcom.2009.02.011

Table 1
The detail of elemental analysis, crystallite size and lattice parameter of calcined ZnO powders at various Fe doping concentrations.

Mol. % Fe in solution	Elemental analysis (at. %)			Crystallite size (nm)	Lattice parameter	
	Zn	Fe	O		a	c
0	55.81	–	43.69	30	0.3250	0.5207
0.01	52.90	0.71	46.39	27	0.3249	0.5206
0.02	57.24	1.10	41.67	25	0.3248	0.5204

2.3. Synthesis of nanocrystalline $Zn_{1-x}Fe_xO$ ($x = 0$, 0.01 and 0.02) powders

0.4 mmol and 0.8 mmol $FeCl_3 \cdot 6H_2O$ were added into the citrate-modified $Zn(NO_3)_2 \cdot 6H_2O$ solution so as to obtain 1 mol. % and 2 mol. % Fe in solution before stirring at 70 °C and adding NaOH solution. The other processes were followed as in preparing nanocrystalline ZnO powders.

2.4. Characterization

The structural identification of calcined powders was carried out using a powder X-ray diffractometer (XRD, Bruker D8 ADVANCE). The Fourier transformed infrared (FTIR) spectrum of calcined powders was recorded on a FTIR spectrophotometer (Elmer FTIR Spectrometer Spectrum 2000). The shape and size of powders were evaluated with a field emission scanning electron microscopy (FESEM, Hitachi, S-4700) and a transmission electron microscopy (TEM, JEOL 2010). The chemical analysis was determined by an energy dispersive X-ray spectrometer (EDS, DMAX). The absorbance was measured in the range of 200–800 nm by a UV–vis spectrophotometer (UV-vis 2450, Shimadzu) and the room temperature photoluminescence (PL) spectra were recorded on a luminescence spectrometer (LS/55, PerkinElmer).

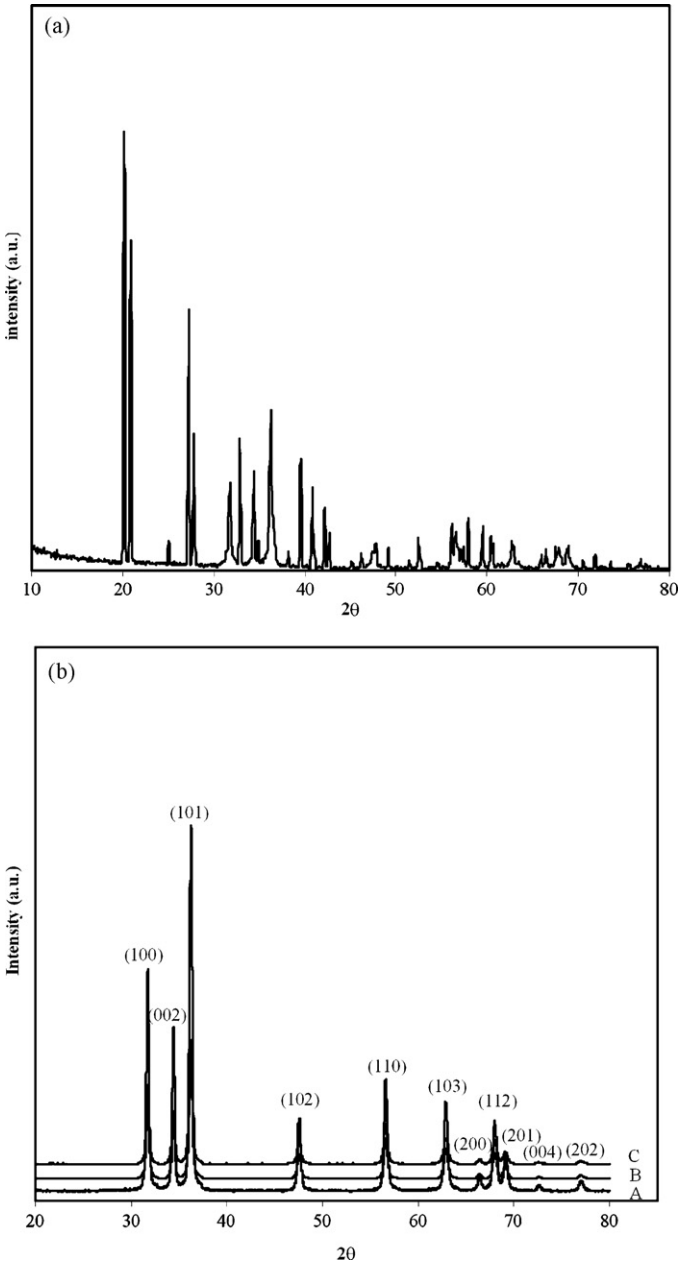

Fig. 1. XRD patterns of (a) as-prepared ZnO powder and (b) calcined powders; A: ZnO, B: $Zn_{0.99}Fe_{0.01}O$ and C: $Zn_{0.98}Fe_{0.02}O$.

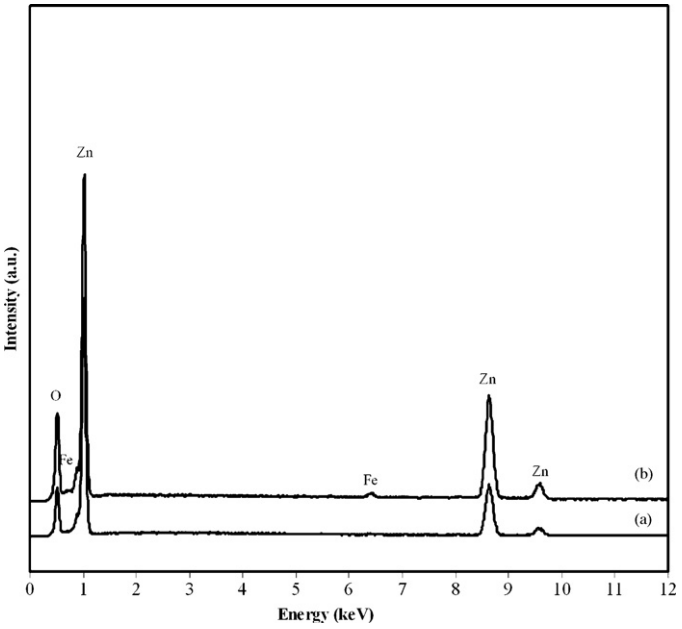

Fig. 2. Elemental analysis of nanocrystalline (a) ZnO and (b) $Zn_{0.98}Fe_{0.02}O$.

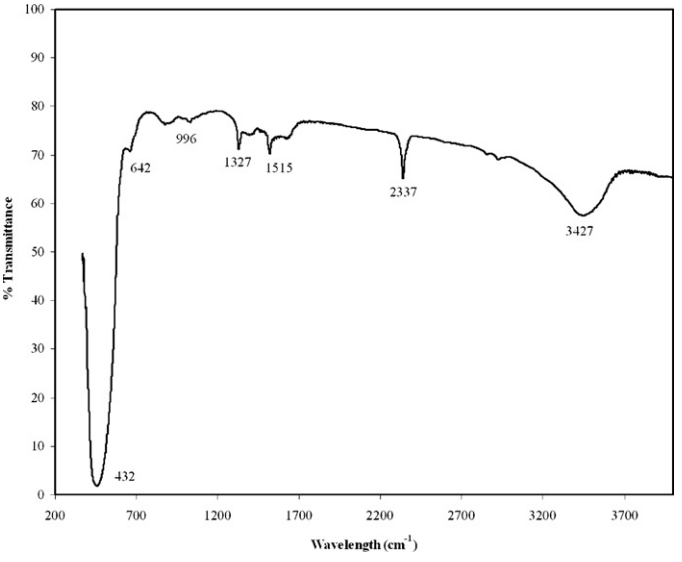

Fig. 3. FTIR spectrum of nanocrystalline $Zn_{0.98}Fe_{0.02}O$ powder.

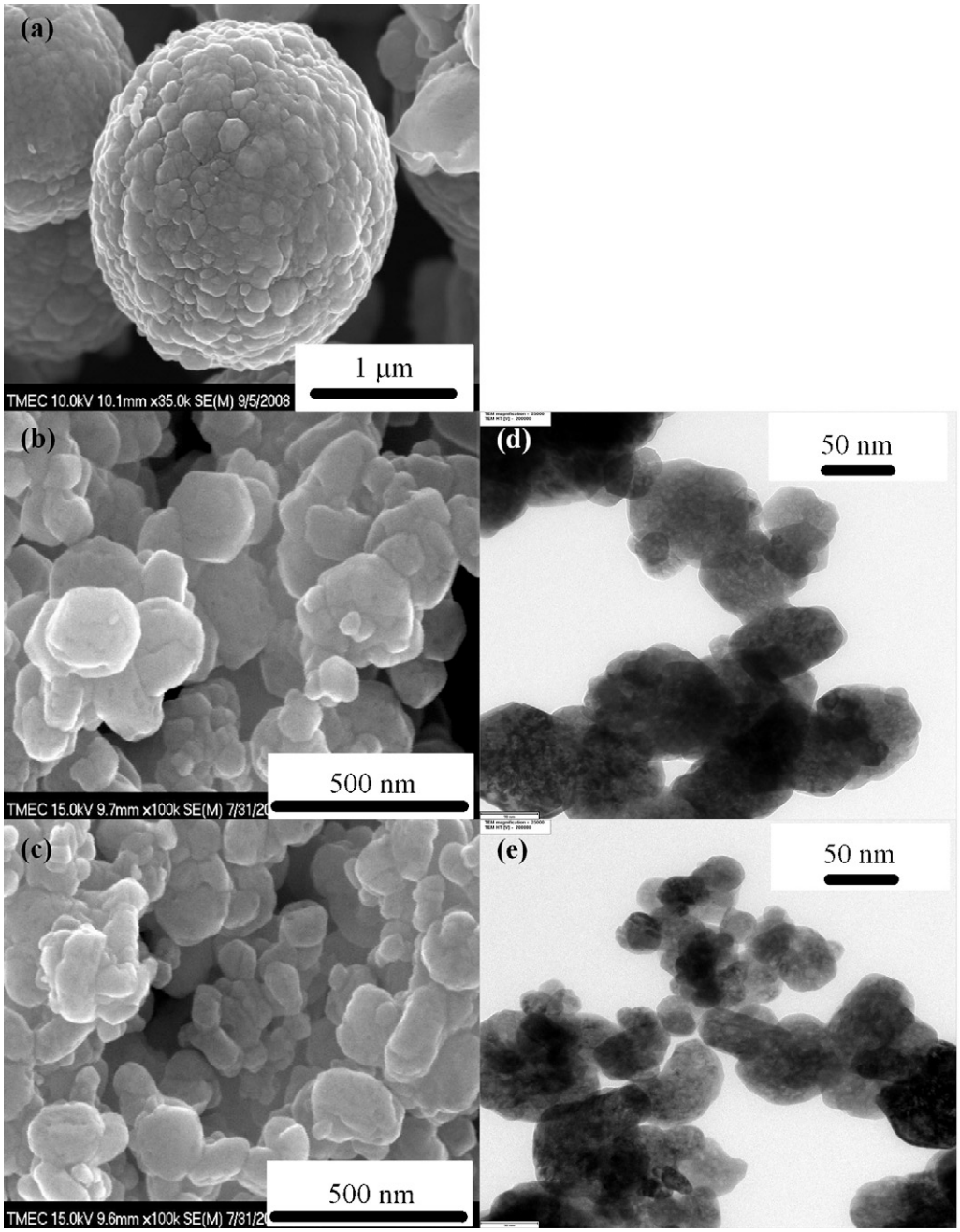

Fig. 4. FESEM images of nanocrystalline (a) ZnO, (b) $Zn_{0.99}Fe_{0.01}O$ and (c) $Zn_{0.98}Fe_{0.02}O$ powders as well as TEM images of nanocrystalline (d) $Zn_{0.99}Fe_{0.01}O$ and (e) $Zn_{0.98}Fe_{0.02}O$ powders.

3. Results and discussion

3.1. XRD analysis

The XRD patterns of undoped and Fe-doped ZnO powders are presented in Fig. 1. In this study, it had been observed that all samples exhibited a hexagonal or wurtzite structure in accordance with the JCPDS database of card number 36–1451 except the as-prepared ZnO powder showed an impurity phase in its X-ray diffraction pattern as seen in Fig. 1 (a). In this investigation, the XRD patterns of calcined ZnO powders showed only diffraction peaks of pure ZnO without any secondary phases such as $ZnFe_2O_4$ and Fe_2O_3 as presented in Fig. 1 (b). Moreover, the peak positions shifted slightly to lower angle as a function of Fe concentrations. This evidence is similar to the effect of a few mol.% Al doped ZnO nanoparticles as reported in [4]. The data refinement showed that the lattice parameter a and c decreased slightly as the Fe concentration was increased because of the smaller ionic radius of Fe^{3+} ion (0.055 nm) comparing to ionic radius of Zn^{2+} ion (0.074 nm), resulting in a contraction of the lattice parameters. From this point of view, it is noteworthy that the Fe ions can substitute for the Zn sites in the wurtzite ZnO structure [9] and the powders are in the form of $Zn_{1-x}Fe_xO$ (where $x = 0$, 0.01 and 0.02) compound.

In order to study the effect of Fe concentrations on a reduction of crystallite size, the crystallite size was evaluated by the Scherrer's formula

$$D = \frac{k\lambda}{\beta \cos\theta}$$

where D is the average crystallite size, λ is the wavelength of Cu Kα, β is the full width at half maximum, K is the constant and θ is the diffraction angle. The calculated crystallite size was presented in Table 1.

It is obvious that the crystallite size decreased as Fe concentration was increased. To prevent a particle growth, the motion of a grain boundary must be impeded [10]. In this study, we can explain the obstruction on a movement of the grain boundaries by Zener pinning. When the moving boundaries attached the zinc interstitial and the substituted Fe ions, they will give a retarding force on the boundaries. If the retarding force was generated more than the driving force for grain growth, the particles cannot grow any longer.

3.2. Composition analysis

Fig. 2 shows the spectra of chemical composition of nanocrystalline ZnO and $Zn_{0.98}Fe_{0.02}O$ powders. It is clearly seen that the chemical composition of nanocrystalline $Zn_{0.98}Fe_{0.02}O$ powders mainly consisted of Zn, O and a trace amount of Fe. The detail of an elemental analysis of all samples was presented in Table 1.

The characteristic FTIR spectrum of nanocrystalline $Zn_{0.98}Fe_{0.02}O$ powders prepared from the citrate-modified $Zn(NO_3)_2{\cdot}6H_2O$ solutions was depicted in Fig. 3. It is evident that the absorption band at 3427 cm^{-1} is due to the hydroxyl stretching mode ν(OH). The absorption peak at 2337 cm^{-1} is because of an existence of CO_2 molecule in air. The absorption peak at 1515 cm^{-1} is ascribed to ν(C═O) and at about 1327 cm^{-1} can be assigned to ν(COO). The absorption peak at 996 cm^{-1} is ascribed to citrate precursor [11] and other two absorption peaks at about 642 cm^{-1} and 432 cm^{-1} are assigned to ν(Fe—O) and ν(Zn—O), respectively [12,13]. In this study, a trace amount of precursor such as citrate ions could strongly adsorb on the ZnO surface, so its adsorption peak was detected by FTIR, while the C-element could not be detected by EDS due to the limitation of this equipment.

3.3. Morphological study

As obviously mentioned in the previous part, the crystallite size of samples decreased as Fe concentrations in the solution or Fe contents in the ZnO structure were increased. In addition, the FESEM and TEM images were performed in Fig. 4 so as to confirm the result from XRD data. It was found that the particle size reduced significantly, the reason was given in a part of XRD analysis. Furthermore, a spherical shape of nanocrystalline ZnO powder was altered to an agglomerated hexagonal-like shape when doping ZnO with Fe ions as clearly seen in Fig. 4 (d) and (e).

3.4. Energy band gap of nanocrystalline $Zn_{1-x}Fe_xO$ ($x = 0$, 0.01 and 0.02) powders

Fig. 5 (a) shows the absorption spectra of nanocrystalline ZnO as well as $Zn_{0.99}Fe_{0.01}O$ and $Zn_{0.98}Fe_{0.02}O$ powders. It is obvious that all powders performed in a highly transparent mode in visible region. Based on the absorption spectra, we can estimate the band gap of all powders from the relationship

$$(\alpha h\nu)^2 = E_D(h\nu - E_g)$$

where α is the optical absorption coefficient, $h\nu$ is the photon energy, E_g is the direct band gap and E_D is the constant. The optical absorption coefficient could be evaluated by the following equation [4]

$$\alpha = \frac{A}{d_s'}$$

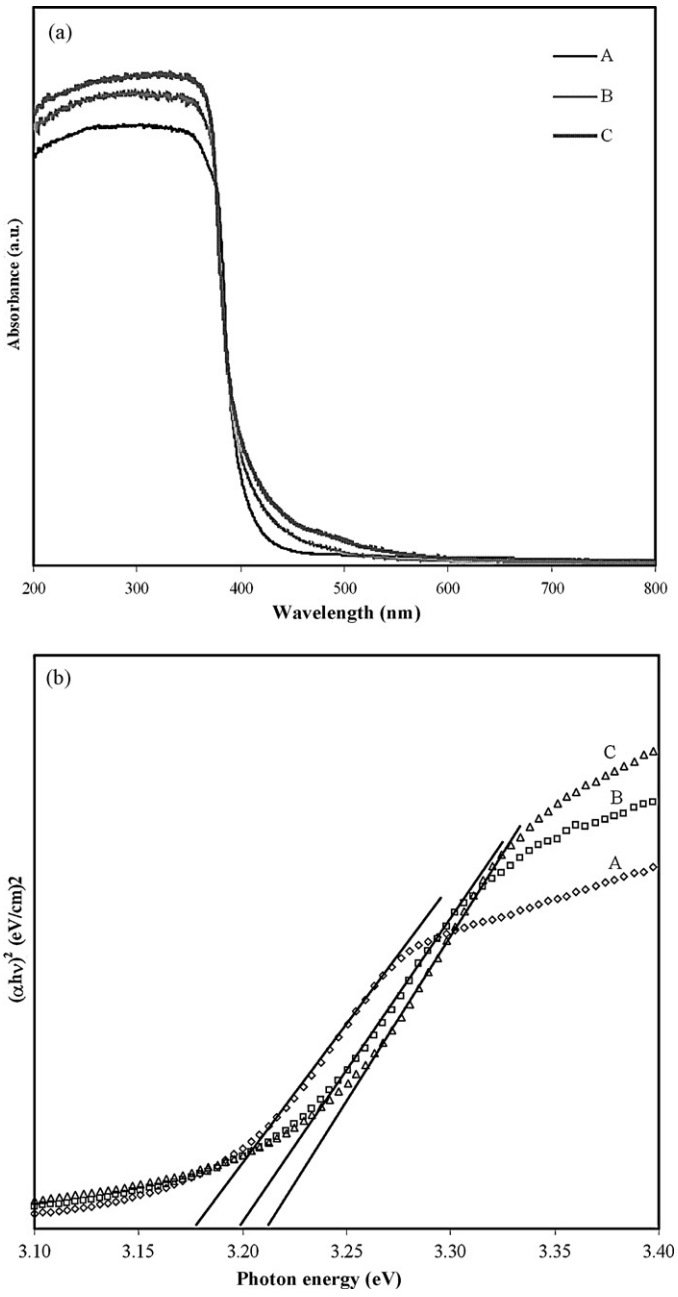

Fig. 5. (a) Absorbance spectra of calcined powders; A: ZnO, B: $Zn_{0.99}Fe_{0.01}O$ and C: $Zn_{0.98}Fe_{0.02}O$, and (b) evolution of the $(\alpha h\nu)^2$ vs. $h\nu$ curves of calcined powders; A: ZnO, B: $Zn_{0.99}Fe_{0.01}O$ and C: $Zn_{0.98}Fe_{0.02}O$.

where A is the measured absorbance and d_s' is the thickness of sample in UV–vis cell.

The linear portion of the graph of $(\alpha h\nu)^2$ versus $h\nu$ when extrapolating to the zero is a direct band gap (E_g) value as presented in Fig. 5 (b). It was noteworthy that the E_g value of nanocrystalline ZnO powders is about 3.170 eV as well as the E_g values of nanocrystalline $Zn_{0.99}Fe_{0.01}O$ and $Zn_{0.98}Fe_{0.02}O$ powders are about 3.195 eV and 3.214 eV, respectively. Although a few researchers [14–16] reported the effect of Fe concentration on the optical band gap of ZnO powders, almost present results manifested that the optical band gap decreased as the Fe concentration was increased. Fortunately, in this study, we were successful in improving the optical band gap of Fe doped ZnO powders by a precipitation method from the citrate-modified $Zn(NO_3)_2{\cdot}6H_2O$ solution. We found that the blue-shift occurred when the Fe concentration was increased. This blue-shift

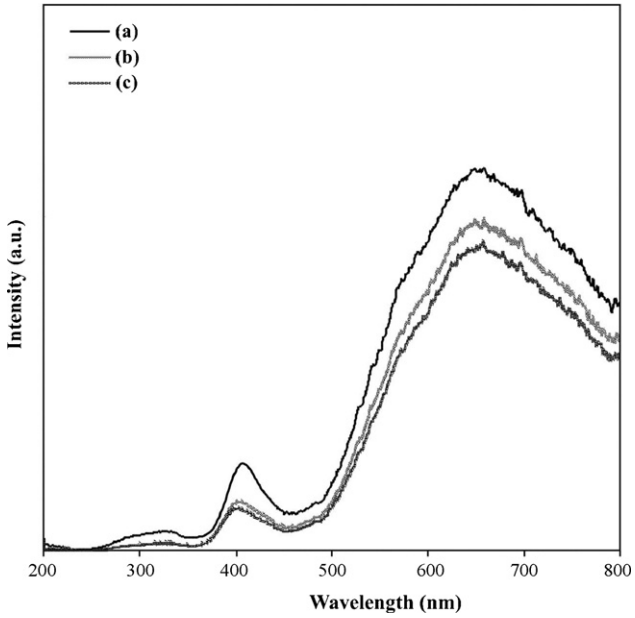

Fig. 6. Room temperature photoluminescence spectra of calcined powders; A: ZnO, B: $Zn_{0.99}Fe_{0.01}O$ and C: $Zn_{0.98}Fe_{0.02}O$.

behavior can in principle be explained by the Moss–Burstein band filling effect as reported in [4,17]. Based on the Moss–Burstein theory, ZnO, $Zn_{0.99}Fe_{0.01}O$ and $Zn_{0.98}Fe_{0.02}O$ powders are an *n*-type semiconductor, the Fermi level will be inside of the conduction band. Since electrons occupy the states below the Fermi level in the conduction band, so the absorption edge should shift to the higher energy or blue-shift.

3.5. Photoluminescence characteristic

Fig. 6 shows the PL spectra at room temperature of nanocrystalline ZnO as well as $Zn_{0.99}Fe_{0.01}O$ and $Zn_{0.98}Fe_{0.02}O$ powders. It is obviously seen that two bands appeared in the photoluminescent spectra, i.e. the near band edge emission that centered at the wavelength below 400 nm originated from the recombination of free excitons through an exciton–exciton collision process. The UV emission slightly shifted to lower wavelength or higher energy with increasing of the Fe concentrations. This shift is in agreement with the results in Fig. 5. Besides, the visible emission (yellow-emission) that centered at about 640 nm is due to the oxygen interstitial (O_i^-). Moreover, it was observed that the PL intensity decreased as Fe concentration was increased. In this study, we could say that a reduction of UV emission intensity of nanocrystalline $Zn_{0.99}Fe_{0.01}O$ and $Zn_{0.98}Fe_{0.02}O$ powders is due to their poor crystallinity comparing to nanocrystalline ZnO powders [18].

4. Conclusion

In present work, nanocrystalline $Zn_{1-x}Fe_xO$ (where $x = 0$, 0.01 and 0.02) powders were successfully prepared from the citrate-modified $Zn(NO_3)_2{\cdot}6H_2O$ solution. All synthetic powders that were calcined at 500 °C for 1 h exhibited the wurtzite structure without the secondary phases. The crystallite and particle size of calcined powders decreased as the Fe concentration was increased. The morphology of the ZnO powder was changed from a spherical shape to a hexagonal-like shape when doping with Fe. For optical studies, the dependence of Fe concentrations on the optical band gap and PL characteristic was elucidated. We found that the optical band gap increased as a function of Fe concentrations because of the Moss–Burstein effect. Moreover, the room temperature photoluminescence of calcined powders showed the UV emission peaks that centered at lower 400 nm and about 640 nm. These UV emission peaks shifted slightly to lower wavelength in concordance with an increase of the optical band gap.

Acknowledgements

This work was funded by the Commission on Higher Education granting. Mr. Tanattha Rattana was supported by Strategic Scholarships Fellowships Frontier Research Networks by the Commission on Higher Education, Ministry of Education, Thailand.

References

[1] J. Liu, X. Huang, J. Solid State Chem. 179 (2006) 843–848.
[2] Y.Q. Huang, L. Meidong, Z. Yike, L. Churong, X. Donglin, L. Shaobo, Mater. Sci. Eng. B 86 (2001) 232–236.
[3] Y.L. Wei, P.C. Chang, J. Phys. Chem. Solids 69 (2008) 688–692.
[4] S. Suwanboon, P. Amornpitoksuk, A. Haidoux, J.C. Tedenac, J. Alloys Compd. 462 (2008) 335–339.
[5] X. Zhou, S. Ge, D. Yao, Y. Zuo, Y. Xiao, Physica B 403 (2008) 3336–3339.
[6] J.H. Yang, L.Y. Zhao, Y.J. Zhang, Y.X. Wang, H.L. Liu, M.B. Wei, Solid State Commun. 143 (2007) 566–569.
[7] H.W. Zhang, Z.R. Wei, Z.Q. Li, G.Y. Dong, Mater. Lett. 61 (2007) 3605–3607.
[8] Z.R. Tian, J. Voigt, J. Liu, B. Mckenzie, M.J. Mcdermott, M.A. Rodriguez, H. Konishi, H. Xu, Nat. Mater. 2 (2003) 821–826.
[9] Y.Q. Wang, S.L. Yuan, L. Liu, P. Li, X.X. Lan, Z.M. Tian, J.H. He, S.Y. Yin, J. Magn. Magn. Mater. 320 (2008) 1423–1426.
[10] R.W. Kelsall, I.W. Hamley, M. Geoghegan, Nanoscale Science and Technology, John Wiley & Sons, 2006, pp. 237–281.
[11] S. Zhan, D. Chen, X. Jiao, S. Liu, J. Colloid Interface Sci. 308 (2007) 265–270.
[12] R. Fu, W. Wang, R. Han, K. Chen, Mater. Lett. 62 (2008) 4066–4068.
[13] Y.Y. Hong, S.Z. Zhang, G.Q. Di, H.Z. Li, Y. Zheng, J. Ding, D.G. Wei, Mater. Res. Bull. 43 (2008) 2457–2468.
[14] Z.C. Chen, L.J. Zhuge, X.M. Wu, Y.D. Meng, Thin Solid Films 515 (2007) 5462–5465.
[15] T. Yogo, T. Nakafuku, W. Sakamoto, S.I. Hirano, J. Mater. Res. 20 (2005) 1470–1475.
[16] Y.S. Wang, P.J. Thomas, P. O'Brien, J. Phys. Chem. B 110 (2006) 21412–21415.
[17] F.K. Shan, Y.S. Yu, J. Eur. Ceram. Soc. 24 (2004) 1869–1872.
[18] M. Wang, K.E. Lee, S.H. Hahn, E.J. Kim, S. Kim, J.S. Chung, E.W. Shin, C. Park, Mater. Lett. 61 (2007) 1118–1121.